RF-AMOC: Human-related RFID Tag Movement Identification in Access Management of Carries

SHAOYI ZHU, Institute of Information Engineering, Chinese Academy of Sciences & School of Cyber Security, University of Chinese Academy of Sciences, China
WEIQING HUANG, School of Computer and Information Technology, Beijing Jiaotong University & Institute of Information Engineering, Chinese Academy of Sciences & School of Cyber Security, University of Chinese Academy of Sciences, China
CHENGGANG JIA, Institute of Information Engineering, Chinese Academy of Sciences & School of Cyber Security, University of Chinese Academy of Sciences, China
SIYE WANG, School of Computer and Information Technology, Beijing Jiaotong University & Institute of Information Engineering, Chinese Academy of Sciences & School of Cyber Security, University of Chinese Academy of Sciences, China
BOWEN LI and YANFANG ZHANG, Institute of Information Engineering, Chinese Academy of Sciences & School of Cyber Security, University of Chinese Academy of Sciences, China

The use of radio-frequency identification (RFID) technology in supply chain has been a fairly mature application in recent years, which can be extended to the field of carrier management for the inventory and access control of sensitive files and mobile storage medium. To address the inherent defects of false readings of RFID, we present RF-AMOC, a tag movement identification system that leverages the signal variation patterns between the opposite antennas and the tag to accurately determine whether someone takes the sensitive carrier out of the room or just the normal carrier usage activity in the room. Particularly, we focus on two kinds of signal variation modes: *Direct side* models, where the RSSI is sensed by one antenna on the tag side, and *obstruction side* models, where the RSSI is sensed by the other antenna that was obstructed by the person. Then, Pearson Coefficient and crest comparison algorithms are adopted to match the theoretical and actual RF-signal curves on the two sides, respectively. Additionally, a starting point acquisition method is proposed to extract the meaningful time period. A prototype of RF-AMOC is realized in two different environments with various persons, and the results validate that it is superior in terms of sensitivity and specificity with strong robustness.

CCS Concepts: • **Human-centered computing** → **Ubiquitous and mobile computing design and evaluation methods**; • **Hardware** → *Sensor applications and deployments*; • **Information systems** → Spatial-temporal systems;

This work was supported by the National Key Research and Development Project under grant 2018YFF0301202.
Authors' addresses: S. Zhu, C. Jia, B. Li, and Y. Zhang, Institute of Information Engineering, Chinese Academy of Sciences & School of Cyber Security, University of Chinese Academy of Sciences, Xingshikou Road, Beijing, China; emails: zhushaoyi@iie.ac.com, {jiachenggang, libowen, zhangyanfang}@iie.ac.cn; W. Huang and S. Wang, School of Computer and Information Technology, Beijing Jiaotong University & Institute of Information Engineering, Chinese Academy of Sciences & School of Cyber Security, University of Chinese Academy of Sciences, Xingshikou Road, Beijing, China; emails: {huangweiqing, wangsiye}@iie.ac.cn.

1550-4859/2020/08-ART33 $15.00
https://doi.org/10.1145/3399678

Additional Key Words and Phrases: RFID, tag movement identification, human-related, carrier security, classification

ACM Reference format:
Shaoyi Zhu, Weiqing Huang, Chenggang Jia, Siye Wang, Bowen Li, and Yanfang Zhang. 2020. RF-AMOC: Human-related RFID Tag Movement Identification in Access Management of Carries. *ACM Trans. Sen. Netw.* 16, 4, Article 33 (August 2020), 23 pages.
https://doi.org/10.1145/3399678

1 INTRODUCTION

The security of sensitive carriers such as files, flash disks, and CDs is a critical issue that has always been of concern and urgently needs to be solved. Take important files as an example, they are generally kept in the room with high security level and can be accessed and viewed in the room (called *"in-room"*). Any unauthorized file taking out behavior (called *"out-room"*) must be strictly prohibited. Meanwhile, there is an imperative need for a means to inventory all files on time to understand the status of files promptly. With the background of the successful application of RFID in the supply chain [5, 6, 22, 31], the above problems seem to be able to find answers from RFID. In an RFID-equipped warehouse, each product is pasted with a unique tag and can be registered automatically when passing through the RFID portal. Similarly, by attaching the RFID tag to each sensitive file and simultaneously deploying monitoring antennas at the door, effective file access control and on-time inventory can be performed. However, the technical and physical limitations of RFID itself may sometimes hinder productive use, the most serious of which is false reading [3]. Specifically, the tag-equipped object detected unintentionally within reading range of the reader is called false positive reading, which is defined herein as mistaken *in-room* as *out-room*. The tag-equipped object that in range seems to be "invisible" to the RFID reader is called false negative reading, which becomes mistaken *out-room* as *in-room* in context. The occurrence of the former situation will produce the false alarm and greatly reduce user satisfaction, while the latter case will lead to serious consequences such as loss of confidential carrier.

In addition to designing better protocols [26, 29], the existing false reading detection solutions are mostly focused on the field of supply chain and can be divided into two categories: (i) Dedicated devices–based approaches require specialized equipment for accurate detection, e.g., modified RFID antenna, acoustic magnetic device, or camera [9, 11, 17, 20, 34, 39], which incur additional expense and are difficult to deploy. Especially, as the most popular camera-based solutions now, though significant progress has been obtained, they still face several challenges such as reliability issues [38] (light and line-of -sight (LOS) restrictions), and the privacy issues (even more serious in sensitive areas). (ii) RF-signal features–based approaches usually exploit received signal strength indication (RSSI) from various aspects. The earliest research used pre-defined thresholds or template RSSI sequences to distinguish "moved" and "static" tags [2, 4, 19, 21]. Nevertheless, the above solutions require an optimal threshold or several template sequences for comparison, which is a relatively subjective matter. More recent works try to solve the false positives based on various machine learning algorithms such as Support Vector Machine (SVM), Logistic Regression (LR), and Neural Network [14, 18, 28]. However, these solutions either require a lot of complicated data collection and training work or do not have strong robustness to adapt to the changes in equipment size and environmental factors. It is conceivable that another effective way to solve the problem of erroneous reading is to accurately locate the tag, which naturally separates the two types of movements by trajectory analysis. The existing RFID localization methods can be roughly divided into two categories: the fingerprint-based approaches and the methods based on signal parameter derivation analysis and model construction. However, the former class of localization approaches

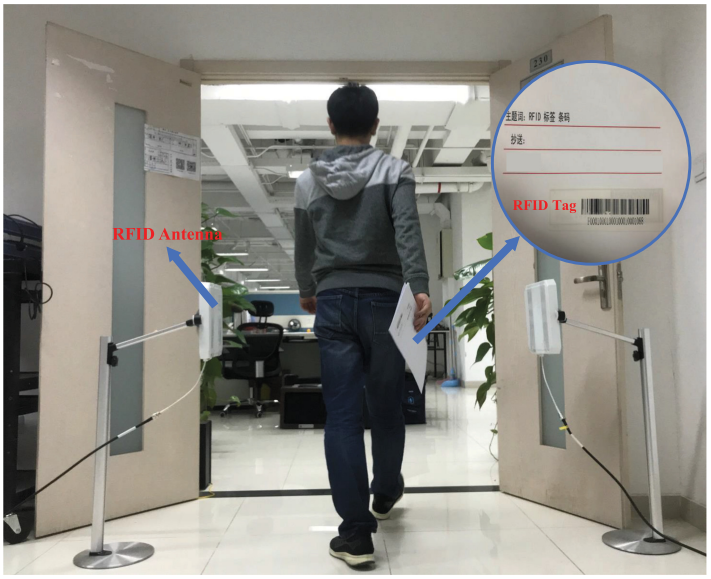

Fig. 1. Illustration of RF-AMOC monitoring system.

[8, 30, 40] also have pain points in the previous data collection and training workload. While the latter class [27, 32] tend to impose strict restrictions on the number or placement of antennas with a relatively large computational burden and limited positioning area, which is troublesome in the practical use of "anywhere, anytime."

Different from the situation that goods in the warehouse move regularly on the conveyor belt or are placed steadily on the shelf, people's activities in the room are dynamic and unpredictable. There are several kinds of *in-room* tag movement trajectories that are similar to the *out-room* ones, the existing methods used in supply chain are not sufficient to accurately distinguish between *in-room* and *out-room* behaviors. As the first research to extend the scenario of solving false reading problem from the supply chain domain to the carrier control field, a general tag movement identification framework based on adjusted self-organizing and incremental neural networks (ASOINN) was proposed [41]. By means of feature extraction and model training, it achieved a sensitivity of over 94% and specificity of over 97%. However, the inaccurate detection results caused by the swinging arms and body occlusion during the *out-room* process become a legacy problem. In fact, swinging arms is the most common action when walking, which cannot be ignored in the human-related tag movement identification scenario. Hence, to make up for this kind of swing-arm situation, we present RF-AMOC, an effective and lightweight RFID tag movement identification system to model the RSSI changes caused by people holding a file walking out of the room with swinging arms. Specifically, as shown in Figure 1, two opposite antennas are placed at the door to constantly monitor whether there is a malicious behavior of carrying file out.

In designing the RF-AMOC system, we face the following three challenging problems: (i) *How do we depict the RSSI variation patterns of two antennas separately with human arms swing and body occlusion considered?* Since people usually hold the file in one hand, when walking out of the door, there is an antenna on the side of the tag, and the antenna on the other side is blocked by the person to some extent. Therefore, the RSSI changes differently between the two opposite antennas and need to be described separately. To address this issue, we first utilize a walking model to depict the relationship between swinging arms with tag displacement. We then regard the person as a

cylinder and construct signal variation models for two antennas based on the attenuation discipline of the signal with distance and angle, taking the human reflection and occlusion effects into account. (ii) *How do we match the theoretical and actual signal curves regardless of some deviation in the RSSI value?* In the actual environment, the existence of the multi-path effect will cause a certain gap between the theoretically calculated RSSI and the actual one, especially for the antenna on the obstruction side. Thus, on the direct side, we use Pearson Coefficient to match the trend of the theoretical and actual RSSI curves, while on the obstruction side, crest comparison algorithm is proposed to better capture and match the undulations of two curves. (iii) *How do we extract the meaningful time period for detection to reduce time consumption and save computing resources?* Considering the efficiency and computing resources, it is not advisable to make judgement all the time. The time periods that cannot be *out-room* should be filtered out directly in the early stage. Thus, based on the Coarse-Grained Filtering (CGF) mentioned in Ref. [25], we leverage "/ – \" trend discrimination method to acquire the starting point of the meaningful time period during which an entrainment event may happen.

The contributions of our work are summarized as follows:

(i) We investigate the tag movement caused by the swing arms while walking and provide two different theoretical models based on the attenuation discipline of the signal with distance and angle for opposite antennas placed at the door.
(ii) We design an RFID-based tag movement identification system, i.e., RF-AMOC, which leverages "/ – \" method to obtain the meaningful time period for detection. In addition, Pearson Coefficient and novel crest comparison method are used to better match the theoretical and actual RSSI curves.
(iii) We implement a system prototype of RF-AMOC with COTS RFID devices and evaluate its performance in two environments with different sizes of doors. The experimental results demonstrate the effectiveness and robustness of RF-AMOC compared with other two state-of-the-art methods.

The remainder of this article is organized as follows: In the next section, some related works will be introduced, followed by preliminaries in Section 3. In Section 4, the main signal variation models are proposed. Then we elaborate on the design detail of RF-AMOC in Section 5 and evaluate its performance in Section 6. Finally, we conclude our work in Section 7.

2 RELATED WORK

Dedicated devices–based approaches: Some previous research and practical applications focus on solving false reading issue based on the dedicated devices, part of which are committed to the improvement of the antenna setups or the alteration of antenna. For example, the detection capability was improved significantly through the setups of three different portals [20]. Alternatively, the specialized antenna with an extremely narrow radiation pattern was designed to minimize the percentage of unwanted reads [11]. Besides, acoustic magnetic or infrared device is also widely studied and partially applied in places such as supermarkets. However, the above solutions either will introduce additional cost or make deployment more difficult. With the widespread use of cameras, computer vision (CV) is combined with RFID to track the individual target in a scene and provide robustness to false positive observations [9, 34, 39]. However, in addition to the inherent defects such as reliability and privacy issue, CV-based solutions cannot solve the problem when the items are hidden purposely or unintentionally.

RF-signal features–based approaches: In the previous work, many researchers tend to leverage RF-signal itself to identify the tag movement and solve the false reading problem. Early studies used the threshold to make judgments, which means if the separate attribute such as reading

frequency, RSSI maximum, mean, and so on, or the combination of attributes is less than the predefined threshold, it will be treated as a false reading and then be filtered out [2, 4]. For more rational threshold selection, information gain criteria was used to determine the optimal discrimination threshold for the indicator to separate the products actually passing through the RFID portal from the products that happened to appear by the portal [21]. Considering that the data generated by reader are not limited to timestamps of individual tag reads, it is better to describe the trend of the signal over a period of time. Thus Dynamic Time Warping– (DTW) based method was proposed to identify tag movement and filter false positives from RFID data stream through more sophisticated time-series analysis techniques [19]. However, the effect of these methods is subject to the selection of the threshold or the template sequences and do not apply to the human-related scenario in this article. Since machine learning has been used widely in different application fields [36], and have shown unique advantages in tasks such as classification and prediction, many researchers have begun to find a breakthrough from this technology to solve the false reading problem. The simple statistical feature was extracted first to distinguish true positives and false positives [14, 18]. To improve detection accuracy, 11 features were extracted utilizing phase and RSSI and then sent to three algorithms, SVM, LR, and DT, for training [28]. The result shows that SVM performed best with accuracy result of over 95% in actual factory cargo data. However, in addition to the shortcomings of complicated previous work, this kind of methods suffer from environmental restrictions, which means changes in the size of the door will affect the effect of system greatly.

As for solving the false reading issue from the perspective of accurately locating the tag, the earliest fingerprint-based approach LANDMARC [30] used a large number of fixed reference tags that arranged with known coordinates to locate the target tag by means of RSSI comparison. To better apply the positioning method to a noisy environment and map the input into the most possible target location, a noise-aware fingerprint localization algorithm [8] that utilizing an innovative adaptive fingerprint Kalman filter (AFKF) was proposed. Furthermore, a multi-direction weight position Kalman Filter [40] was designed to combine the RSSI data from four different directions, which achieved the localization error of 16cm. However, many researches tend to establish a signal model and obtain the final position by solving multiple equations. For example, the phase difference was used to derive the distance difference between the tag and the two antennas, thereby forming a positioning model based on the hyperbolic intersection and achieved the mean accuracy of 12.8 cm with variance of 3.8 cm [27]. PATL [32] takes advantage of a latest RFID device that equipped with 52 phased array antennas to scan the surveillance region in turns, and the tag was located at the centroid of the quadrangle that formed by the centers of different beams. However, the above approaches are either plagued by the huge pre-workload or require precise antenna numbers and placement rules, which makes them difficult to deploy for practical use. Therefore, our work focuses on adopting a relatively lightweight false reading detection approach that does not require the accurate location of the tag all the times, which also eliminates the need for heavy computational burdens and special device deployment.

3 PRELIMINARIES

The signal indicators that can be acquired from the RFID device typically include RSSI, phase, and Doppler shifts. Among them, the Doppler shifts obtained from the API is generally too noisy to use directly [12]; phase is a more sensitive indicator than RSSI and is often used to perceive small-scale, fine-grained gestures. To figure out how the signal changes caused by tag movement during the *out-room* process, we first explain the reasons for adopting RSSI rather than phase to build the model, and then we conduct preliminary studies on the impact of distance, angle, and the human occlusion on RSSI. Based on these observations, we can model the RSSI variation patterns of two antennas for designing the system.

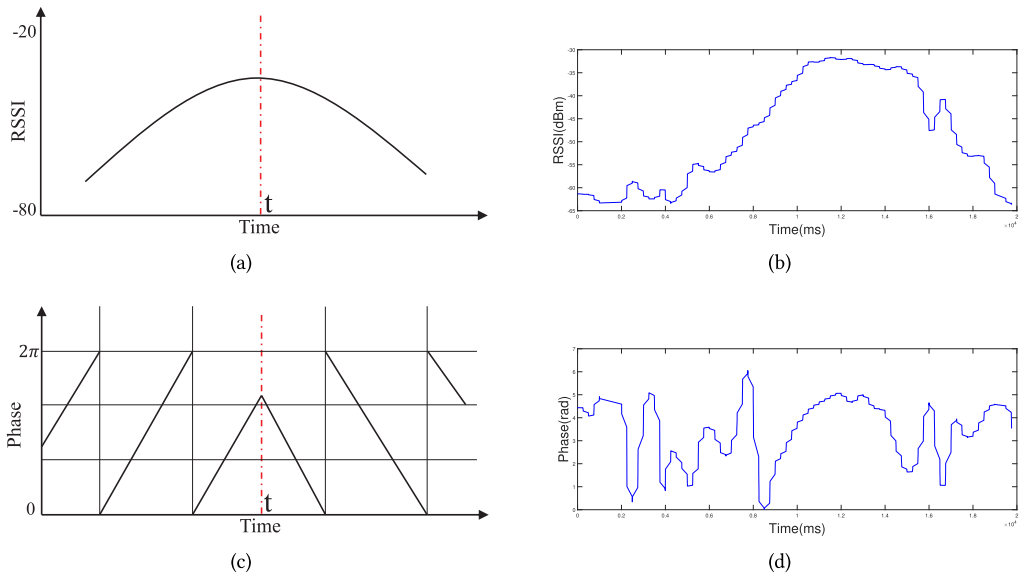

Fig. 2. The signal curves of (a) theoretical RSSI, (b) real RSSI, (c) theoretical phase, and (d) real phase.

3.1 Selection of Signal Parameter

Theoretically, the *out-room* motion is the process of getting close to the antenna and then getting away from it, "t" is the time to reach the position that right opposite the antenna. Therefore, the RSSI will show a trend of becoming larger first and then getting smaller, symmetrically centered on "t" (called *"inverted V pattern"*), as shown in Figure 2(a). As for the phase, within one wavelength, the phase changes from 0 to 2π linearly with the distance and then drops abruptly to 0 for the next cycle [28]. Similarly to RSSI, the change of phase also shows symmetry centered on "t" [35], as shown in Figure 2(c). To verify the availability of the theoretical signal patterns, we collected the RSSI and phase data of the tag as it passed in front of the antenna in a straight line from left to right at a constant speed, the change curves are shown as Figure 2(b) and Figure 2(d).

An insight derived from the figures is that the real *out-room* RSSI curve is basically consistent with the theoretical one, which is intuitive and easy to describe. As for the phase, although the periodicity and symmetry of the curve can be roughly observed, there are many unexpected fluctuations due to its sensitivity to the dynamics, which will increase the difficulty of pattern extraction. Moreover, the situation in the Figure 2 is only for the case where the tag passes relatively evenly without any occlusion and shaking, it is harder to capture the phase discipline when the swing of the arm and the occlusion of the body are introduced. Thus, considering that the *out-room* process is a relatively coarse-grained motion and a lightweight curve trend description way to discriminate the movement of tag is more appropriate, we discard phase and choose RSSI with clearer change pattern for subsequent processing.

3.2 Impact of Distance and Angel on RSSI

3.2.1 RSSI Attenuation with Distance. In the absence of electromagnetic interference, the transmission loss of electromagnetic waves follows log-distance path loss model [1]:

$$PL(d) = \overline{PL(d_0)} + 10n_p \lg\left(\frac{d}{d_0}\right) + X_\sigma, \tag{1}$$

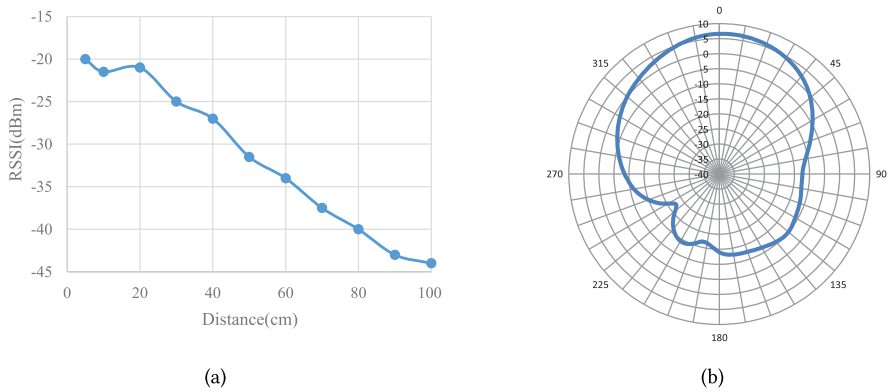

(a) (b)

Fig. 3. RSSI change discipline with (a) distance and (b) angle.

where PL (d) is the measured path loss at distance d and PL (d_0) represents the path loss at d_0. n_p denotes the environmental factor that fluctuates between 2 and 4, and X_σ is the ambient noise conforms to normal distribution, which is relatively small compared with $\overline{PL\,(d_0)}$ [15]. Then, according to Equation (2), the received signal strength $\mathrm{P_r}\,(d)$ in the distance of d can be formulated in Equation (3), where P_t denotes the power intensity of the transmitted signal,

$$P_r\,(d) = P_t - PL\,(d)\,, \tag{2}$$

$$P_r\,(d) = \overline{P_r\,(d_0)} - 10n_p \lg\left(\frac{d}{d_0}\right) - X_\sigma\,. \tag{3}$$

Theoretically, the RSSI decreases with increasing distance and conforms to the logarithmic model based on Equation (3). However, there may be some fluctuations in the RSSI value due to the existence of reflection, occlusion, and the multi-path effect in the real environment, as shown in Figure 3(a). In fact, the multi-path effect can be avoided as much as possible by adopting some strategies on the antenna deployment, frequency setting and data preprocessing [16]. For example, the quality of line-of-sight can be basically ensured in the process of *out-room*, which helps reduce the multi-path effect. Second, the channel hopping mechanism of RFID is also beneficial for this problem. Third, utilizing some denoising method such as the DWT-based approach will impair the impact of excessive noise in the data processing module.

3.2.2 RSSI Attenuation with Angle. The prototype of RF-AMOC consists of a reader with two RFID antennas. The radiation pattern of the antenna in H plane is shown in Figure 3(b). To get the specific relationship between RSSI attenuation and angle, we fit the radiation pattern data within 180° in front of the antenna and get the following function:

$$R\,(\theta) = -0.0020140^2 - 0.0009455\theta - 0.3127 \tag{4}$$

where $R\,(\theta)$ is the loss when the angle between two positions that equidistant from the antenna is θ, $(\theta \in [-90, 90])$, one of which is directly opposite the antenna. Therefore, combining Equation (3) and Equation (4), the RSSI values of all positions in front of the antenna can be obtained from Equation (5),

$$P_r(d, \theta) = \overline{P_r(d_0, 0)} - 10n_p \lg\left(\frac{d}{d_0}\right) + R\,(\theta)\,. \tag{5}$$

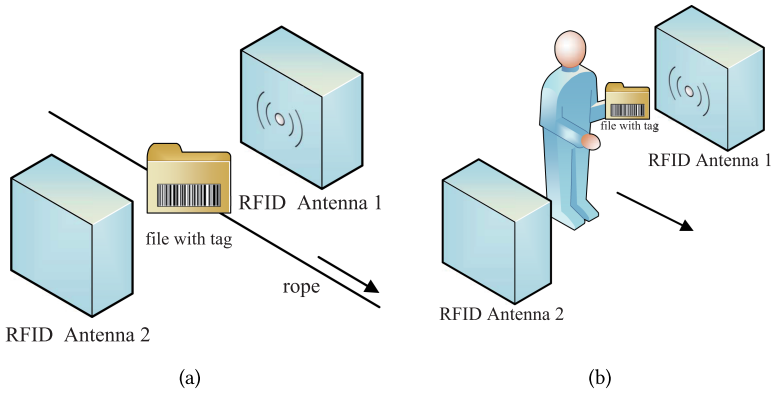

Fig. 4. Preliminary study of RSSI change patterns that the file (a) hanging on the rope and (b) hold in hand.

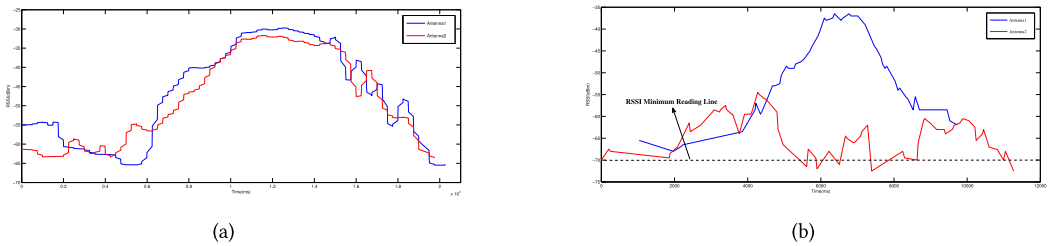

Fig. 5. RSSI variation of two antennas with (a) no person involved and (b) the person walking out without swinging arms.

3.3 Impact of Human Occlusion on RSSI

To systematically study how to use the two opposite antennas to model the tag movement when people walking out of the room, we first conduct a controlled experiment to analyze the influence of human existence on the RSSI. Specifically, as shown in Figure 4(a), the tag-equipped file is hung on a rope passing through the door slowly with the cooperation of the people on two sides. The RSSI values during this period are shown in Figure 5(a), through which we can clearly see that when no one is involved in the *out-room* behavior of the tag, the signals collected by two antennas are basically consistent.

Additionally, when we hold the file walking out without swinging arms as Figure 4(b), we can observe from Figure 5(b) that the relationship between the values of the two antennas has changed. Although both antennas have similar signal variation disciplines with the inverted V pattern, the RSSI amplitude of antenna on the obstruction side (Antenna 2) is obviously lower then the direct side one (Antenna 1), which indicate that a large part of the signal energy is attenuated due to human blockage. Therefore, we need to model the two antennas separately in Section 4. Moveover, the RSSI readings on the obstruction side fluctuate between −70 and −75, thus we set the *RSSI Minimum Reading Line* to −70 dBm.

4 UNDERSTANDING THE TAG MOVEMENT VIA OPPOSITE RFID ANTENNAS

4.1 Modeling the Tag Displacement When Walking

Since the RSSI value is closely related to the distance and angle from the antenna, we first need to model the displacement of the tag with time when walking out of the room, which is equivalent to the movement of the hand that holding the file. In this work, we consider that the person walks

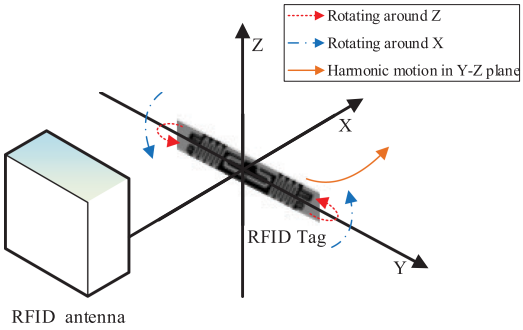

Fig. 6. Tag's movement and rotation in *out-room*.

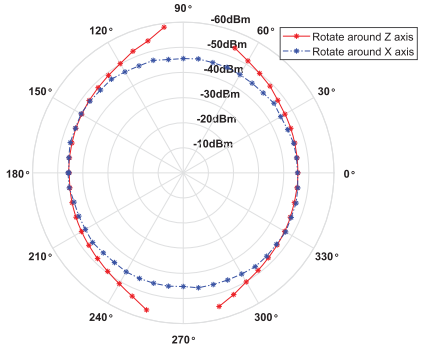

Fig. 7. RSSI variation when rotating around the Z- and X-axes.

at a constant speed and the swing of arms conforms to the principle of the pendulum, which is a simple harmonic motion. Thus, the movement of the tag is mainly a harmonic motion in the Y-Z plane plus rotation around the X-axis in small range, as shown in Figure 6. In addition, the slight rotation around the Z-axis may be introduced due to the habitual motion of the hands. To illustrate the effect of tag's rotation on RSSI, we rotate the tag around the Z and X axes for one cycle while fixing its distance to the antenna, respectively. We observe from the Figure 7 that when the tag rotates around the X-axis, the overall RSSI fluctuation range is small, which is within 3 dBm including the measurement error. When the tag rotates around the Z-axis, the RSSI value decreases as the angle of rotation increases, and it is almost unreadable when the tag rotates to point at the antenna (along the X-axis). The reason behind this is that the angle between the tag polarized direction and the tag-to-antenna direction is almost constant when the tag rotates around the X-axis, while it changes continuously with the tag's rotation around the Z-axis [16]. Considering that the rotation around the Z-axis is faint (generally less than 30°) during the movement of the tag, which does not cause much RSSI change in Figure 7. Therefore, it can be inferred that neither of the above two kinds of rotations will have much impact on results, and only the harmonic motion in the Y-Z plane plays a decisive role in RSSI value.

Besides, we find that the forward swinging amplitude is always greater than the backward amplitude in actual observation. Although the swing amplitude is not fixed for different people, the disparity is small and will not have much impact on the result, thus the uniform setting here is 0.6 m for the front swing and 0.25 m for the backswing. According to Equation (6), let Sf be the stride length, v is the speed of walking, the walking cycle T can be calculated as:

$$T = \frac{2Sf}{v}. \tag{6}$$

Then we define two sine functions to represent the forward-backward swinging process as Equation (7) and combine them to produce a complete formula for tag displacement X over time t as Equation (8),

$$s_1 = 0.6 \sin\left(\frac{2\pi t}{T}\right), s_2 = 0.25 \sin\left(\frac{2\pi t}{T}\right), \tag{7}$$

$$X(t) = s_1.(s_1 \geq 0) + s_2.(s_2 \leq 0) + vt. \tag{8}$$

As an example, we select $v = 1.0$ m/s and $Sf = 0.7$ m and plot $X(t)$ as shown in Figure 8. It is found that when the arm is swinging forward, the displacement of the tag is much greater than person's, and when the arm is swinging backward, the total displacement of it is still moving

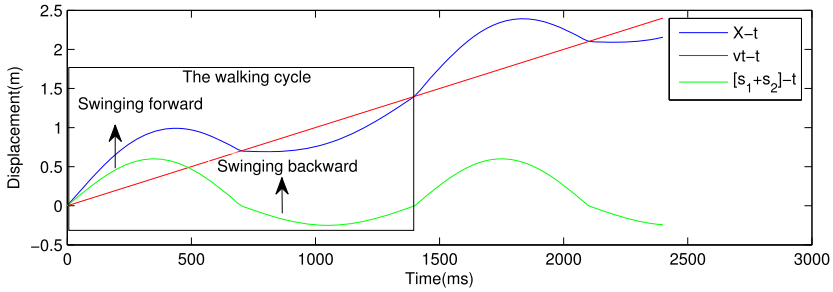

Fig. 8. Illustration of tag displacement *X(t)*.

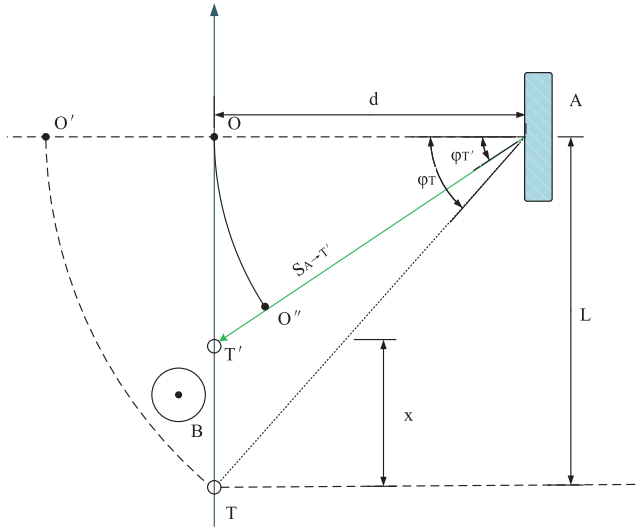

Fig. 9. RSSI model on direct side.

forward slowly. The essential reason is that although the tag itself is retreating relative to the person, person's forward displacement becomes leading cause at this moment.

4.2 Modeling RSSI on Direct Side

To understand how the tag movement affects the signal of the antenna on the direct side, we use the signal propagation model discussed before together with tag displacement to depict the RSSI variation pattern. As shown in Figure 9, A, T, B denote the RFID antenna, RFID tag and person, respectively. Because there is no obstruction between the antenna and the tag on this side, and the reflection caused by the human body is also small, thus we only consider the line-of-sight(LOS) signal here. Assume that the initial positions of the person and the tag are known, the vertical and horizontal distances of the tag to the antenna are L and d, respectively. When the person continues to move and drives the tag forward $x = \int_0^{t_1} X(t)$ to T', the signal propagation path changes from $d_{T\to A}$ to $d_{T'\to A}$, which are the hypotenuse of two triangles ΔTAO and $\Delta T'AO$. Let $\varphi_T = \arctan(\frac{L}{d})$ and $\varphi_{T'} = \arctan(\frac{L-x}{d})$ donate the angle $\angle TAO$ and $\angle T'AO$.

Assume O is the projection of A on the trajectory line of T, and making an arc from T and intersecting the line AO at O'. Since we can get RSSI of the tag in initial position T as P_r^T, then the

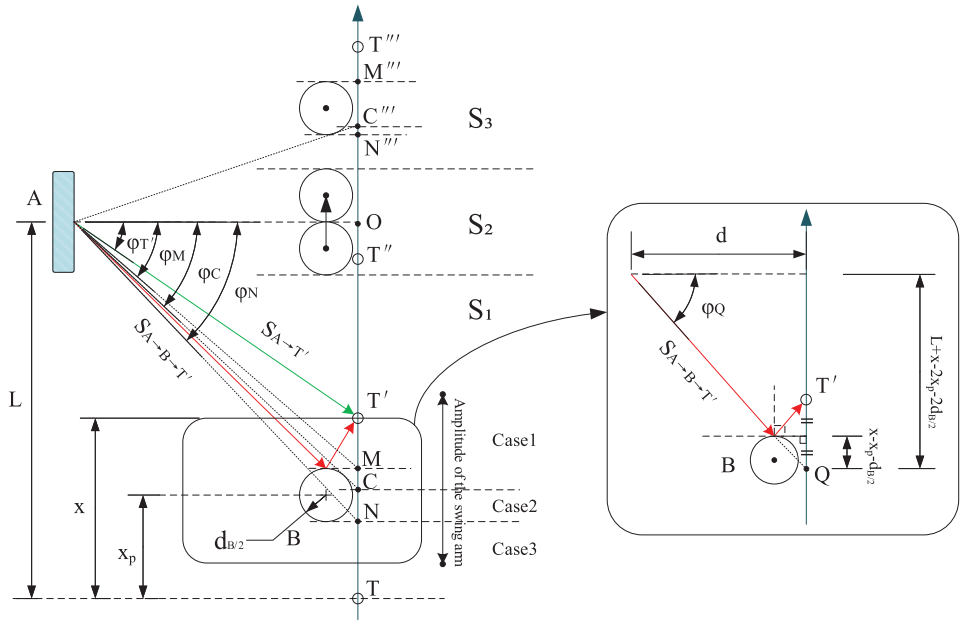

Fig. 10. RSSI model on obstruction side.

RSSI value in O' is

$$P_r^{O'} = P_r^T - R(\varphi_T) \tag{9}$$

Then, we can obtain the RSSI value in O as

$$P_r^O = P_r^{O'} - 10n_p \lg\left(\frac{d}{d_{T\to A}}\right) = P_r^{O'} - 10n_p \lg\left(\frac{d}{\sqrt{d^2+L^2}}\right). \tag{10}$$

Similarly, by making an arc from the O and intersecting the line AT' at O'', we can further get the RSSI value in T':

$$P_r^{T'} = P_r^O + R(\varphi_{T'}) - 10n_p \lg\left(\frac{\sqrt{d^2+(L-x)^2}}{d}\right). \tag{11}$$

Given the initial position of the tag and its RSSI, we can calculate the RSSI values of the *out-room* process from this starting point from Equation (11) and then form a theoretical RSSI curve. Note that the speed and the stride length vary with different people, and cannot be determined by simply fixing a value, which means if the value used in the theoretical calculation differ widely from the actual one, the subsequent curve matching will be in trouble. The solution is that we make multiple curves at a certain resolution within the normal range of speed and stride, which will be further discussed in Section 5.

4.3 Modeling RSSI on Obstruction Side

In regard to the signal of the antenna on the obstruction side, it is essential to take into account the reflected signal and shielding effect caused by the person. Without loss of generality, we consider the person as a cylinder with a radius of $d_{\frac{B}{2}}$ to study its impact on signal propagation. As shown in Figure 10, let $x_p = \int_0^{t_1} vt$ be the displacement of the person, we divide the whole process of *out-room* into three areas, namely inside the door (S_1), in front of the door (S_2), and outside the

door (S_3), respectively. Besides, since the amplitude of the arm swing is generally greater than the width of the body, there will be three cases for the positional relationship between the antenna, the person and the tag. Next, we separately analyze the changes in the signal for different areas and different cases.

4.3.1 S_1. $L - x_p - d_{\frac{B}{2}} > 0$. In the area of S_1, the person is walking toward the door, and the relative positions of the antenna, the person and the tag are constantly changing with the arm oscillates. To clarify how this kind of relationship influence the signal, two horizontal tangent lines of the cylinder are made to intersect the trajectory line of the tag at point M and N, and a tangent line of the cylinder from the antenna intersects the trajectory at point C. Considering that the outer contour of the person is tangent to the trajectory of the tag, the horizontal distance between the person and the tag is very close. Thus, let $\varphi_C \approx \varphi_M = \arctan(\frac{L-x_p-d_{\frac{B}{2}}}{d})$ and $\varphi_N = \arctan(\frac{L-x_p+d_{\frac{B}{2}}}{d})$ donate the angle $\angle CAO$ and $\angle NAO$.

Case 1: $\varphi_{T'} \leq \varphi_C$. In this situation, the tag is located in a position that can communicate directly with the antenna without being affected by the human body at all. Moreover, the person is now equivalent to an intermediate reflectors among the antenna and the tag, the signal that T' received is a superposed one contains LOS signal and the reflection signal from the person B (regardless of the reflection of the surrounding environment), which can be represented as:

$$S_{T'} = S_{A\to T'} + S_{A\to B\to T'}. \tag{12}$$

The RSSI of the direct signal $S_{A\to T'}$ that scattered back to the antenna by the tag can be obtain based on Equation (11), expressed as $P^{T'}_{r,d}$. As for the reflection signal $S_{A\to B\to T'}$, we first extend the line AB and intersect the trajectory line of the tag at point Q and define $\angle QAO$ in Equation (13), then the RSSI of it $P^{T'}_{r,r} = P^{Q}_{r}$ can be acquired according to Equation (11) similarly,

$$\varphi_Q = \arctan\left(\frac{L + x - 2x_p - 2d_{\frac{B}{2}}}{d}\right). \tag{13}$$

Finally, the total RSSI that obtained by mixing the two kinds of signals can be calculated by the signal power superposition formula:

$$P^{T'}_{r,all} = 10\lg\left(10^{\frac{p^{T'}_{r,d}}{10}} + 10^{\frac{p^{T'}_{r,r}}{10}}\right). \tag{14}$$

Case 2: $\varphi_C < \varphi_{T'} \leq \varphi_N$. When the position of the tag relative to the human body is within the width of the body, the propagation of the signal is gradually hindered as the arm continues to swing backward, resulting in a decrease in RSSI. In addition, the reflected signal of the person is difficult to reach the tag in this case due to the inappropriate angle. Therefore, the signal that T' received will be an attenuated direct signal $S'_{A\to T'}$ in Equation (15). Since the duration in this case is relatively short, the attenuation can be set to a fixed value, and the reduced RSSI is formulated in Equation (16),

$$S'_{A\to T'} = S_{A\to T'} - \gamma, \tag{15}$$

$$P^{T'}_{r} = P^{T'}_{r,d} - P^{\gamma}_{r}, \tag{16}$$

where γ is the signal attenuation, and the RSSI reduction P^{γ}_{r} is set to 8 dBm here on the basis of the experimental results.

Case 3: $\varphi_{T'} > \varphi_N$. It is intuitive to discover that when the positional relationship of the three belongs to this case, the signal is difficult to reach tag or scatter back to the antenna, which means even if there is a few small readings appearing occasionally, the RSSI value will be comparatively

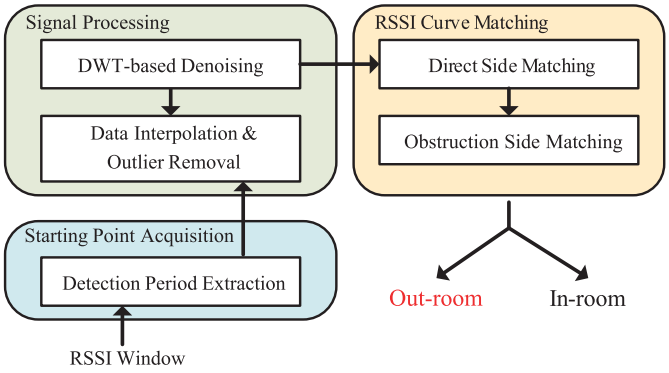

Fig. 11. Overview of RF-AMOC.

small and the interval between readings will be long due to the unstable propagation. Hence, to facilitate subsequent curve comparison, we set RSSI to −70 dBm according to the *RSSI minimum reading line* in case of occlusion in Figure 5(b).

4.3.2 S_2. $L - x_p - d_{\frac{B}{2}} \leq 0, L - x_p + d_{\frac{B}{2}} \geq 0$. When the person moves to this area, he arrives at the closest position to the antenna, which means that although the relative position of the tag and the antenna is also the closest, the signal will be greatly disturbed by the person. Moreover, the duration in S_2 is short, unnecessary fluctuations in RSSI values will be introduced if three cases are subdivided, resulting in some troubles in subsequent curve matching. We thus use the attenuated direct signal $S'_{A\to T''}$ to calculate the RSSI $P_r^{T''}$ according to Equation (16).

4.3.3 S_3. $L - x_p + d_{\frac{B}{2}} < 0$. The situation in the S3 area is actually symmetrical with S1, where $\varphi_{T'''}$, $\varphi_{C'''}$ and $\varphi_{N'''}$ all become negative, which means **Case 1** here refers to $\varphi_{T'''} > \varphi_{N'''}$, while **Case 2** corresponds to $\varphi_{C'''} < \varphi_{T'''} \leq \varphi_{N'''}$ and **Case 3** is $\varphi_{T'''} \leq \varphi_{C'''}$.

5 RF-AMOC SYSTEM DESIGN

5.1 System Overview

The major objective of our work is to identify the tag movement to avoid the occurrence of false readings. Toward this end, we design RF-AMOC, an automatic monitoring and discriminating system consisting of three main components: *Starting Point Acquisition*, *Signal Preprocessing* and *RSSI Curve Matching*, as shown in Figure 11. Specifically, the system takes the time window that containing a series of RSSI values for two antennas received from the tag as input. The *Starting Point Acquisition* separates the signals from the two antennas and detects the starting point of the activity period for the following judgment. After the meaningful time period is acquired, *Signal Preprocessing* first calibrates the RSSI by interpolating the misreading values and removes the outliers through the Hampel Identifier algorithm [23], then Discrete Wavelet Transform (DWT) is used to further reduce the ambient noise. Next, *RSSI Curve Matching* generates two theoretical RSSI curves and compares them with the actual curves using the Pearson Coefficient and crest comparison method. If two pairs of curves both match successfully, then the behavior in this window is considered as the *out-room* one.

5.2 Starting Point Acquisition

For efficient detection, one of the key problems in this system is to filter out activities such as standing still or walking randomly in the room and find the meaningful time period in which an

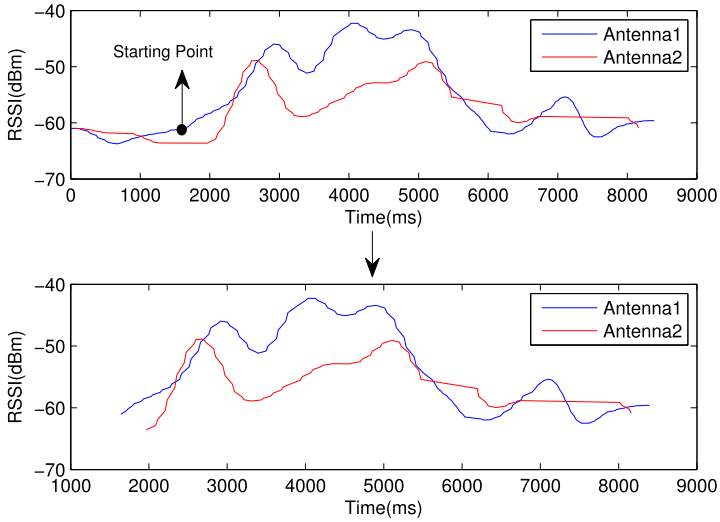

Fig. 12. The effect of starting point acquisition.

entrainment *out-room* event may happen. Thus, it is essential to locate the starting point of the *out-room* process, which refers to the moment when the arm holding the file is swinging forward here. During the half cycle of swinging the arm forward and then back to the side of the body, the distances between the tag and the two antennas both become smaller first and then larger according to Figure 8, which causes the RSSI present the inverted V pattern. However, because of the heterogeneity of the antenna, the undulations of the two antennas are not necessarily exactly the same, and there may be a delay in time. Hence, we need to describe this undulate process and develop a strategy to capture the starting point. Specifically, drawing on the CGF [25], which was proposed to roughly match the phase profile by classifying the variation trend into three states, we divide the trend into three types of symbols: increase (/), stable (−), decrease (\). Any curve can be explained with the combination of the three symbols, e.g., for the half cycle of swinging arm mentioned above, the RSSI trend of both antennas can be described as "/ − \", or "/\." Based on the above definition, a sliding window with 50% overlap is used to continuously scan the RSSI changes. Consider the two antennas in a window w separately as follows: The average RSSI changes λ within w is first calculated, then for each RSSI difference δ_i between the current and the previous samples, if $\delta_i > \lambda$, we record the symbol is "/"; otherwise, we record it as "\" if $\delta_i < -\lambda$, or "−" if $-\lambda \leq \delta_i \leq \lambda$. We can simplify the series of trend symbols of w and get a streamlined sequence according to the rules below:

- Remove extra "−" at the beginning and the end of the series.
- Remove the "−" between two identical symbols.
- Combine adjacent symbols into one if they are the same.

For example, the initial sequence is "− − / − −\−", which becomes "/ − \" after the above operations. Thus, two simplified symbol sequences can be obtained for two antennas in w, and only if the two sequences both $\in$ {"/","/\","/ − \"}, the first point in first "/" is the starting point of the detection period. It can be observed from Figure 12 that the starting point is acquired accurately through this method, and 4 s from the starting point is defined as a meaningful time period D for further detection.

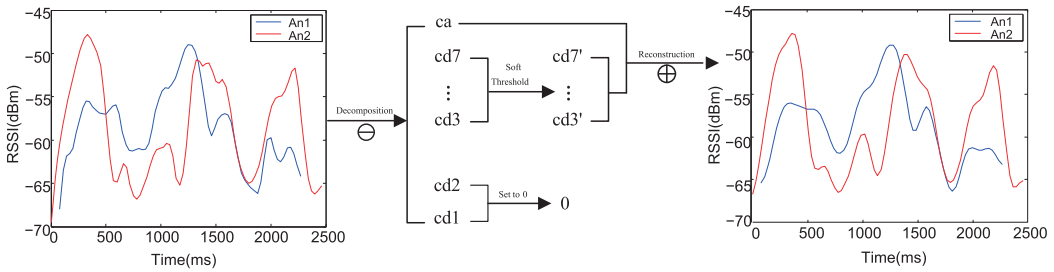

Fig. 13. DWT denoising flow.

5.3 Signal Preprocessing

After getting the detection interval D, we first need to preprocess the RSSI values in it, which contains 3 parts: *Interpolation*, *Outliers removal*, and *Denoising*. The COTS RFID system follows EPC Gen2 standard [33] to challenge the tag randomly, which causes the consequence of uneven sampling. To tackle this problem for better curve matching, Cubic Spline Interpolation [7] is adopted to evenly arrange data with a spacing of 50 ms. Moreover, some outliers might appear due to the inherent defects of the instrument itself or the noise of the environment. To avoid the adverse effects of these outliers, we use Hampel Identifier [24] to remove this kind of points and obtain a "pure" RSSI sequence.

Considering that the theoretical curve is smooth and the appearance of each crest (trough) is the result of the relative positional change of the antenna, person and the tag, which is a reasonable matter. However, in addition to these obvious crests and troughs, there are some small fluctuations existing in the actual curve due to the multi-path effect from the environment or the fine-grained movements from the human. The existing denoising methods can be divided into two categories: time domain, frequency domain. The approaches in time domain such as median filtering and Principal Component Analysis (PCA) denoising [13] tend to lose important high frequency information, while the approaches in frequency domain such as low-pass, high-pass and band-pass filtering remove out-of-band noise only. In view of the above methods, DWT seems to be more suitable for further noise reduction in both time and frequency domain [37].

The procedure of DWT is divided into three steps: decomposition, filtering, and reconstruction. The signal is first decomposed into seven levels utilizing coif5 as the mother wavelet. Then the approximation coefficients *ca* and seven sequences of detailed coefficients *{cd1,cd2,...,cd7}* with decreasing frequency can be obtained for the next step of filtering. Since *{cd1,cd2}* have higher frequency that corresponding to noisy signal, we remove them directly. In regard to the other components, we use the soft threshold function to handle them based on our experimental results. Finally, the signal is reconstructed by reversing DWT with combined *{ca,cd3',...,cd7'}*. As shown in Figure 13, the leftmost graph is the result of the interpolation and outliers filtering. Note that after DWT denoising, the main crests and troughs of the curve are preserved, while the small fluctuations caused by noise are reduced.

5.4 RSSI Curve Matching

After preprocessing the actual signal curve in D, the next step is to match it to the theoretical one constructed in Section 4. Because of the difference in signal variation patterns on both sides, the matching method adopted for one antenna should be differ from another.

5.4.1 Pearson Coefficient–based Matching on Direct Side. Since the theoretically calculated RSSI value has an unpredictable gap with the actually measured one, some curve similarity measure

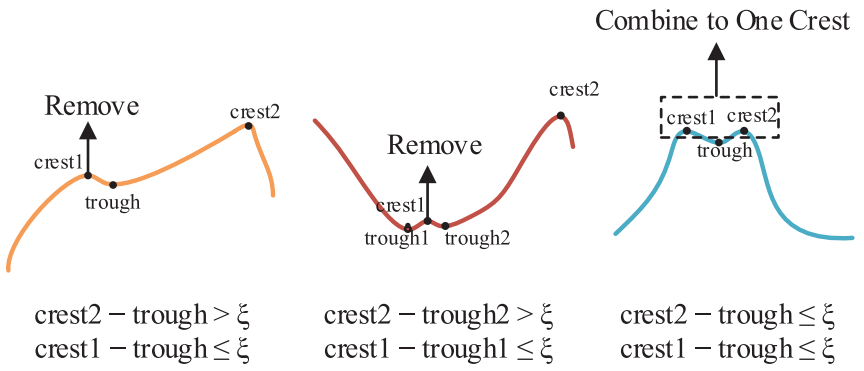

Fig. 14. Filtered "small" crests.

methods that are very relevant to absolute value are no longer applicable, such as the method based on Euclidean Distance. Besides, Dynamic Time Warping (DTW) is widely used to compare the similarity of two time series that may not be equal in length [10]. However, it is difficult to have an objective criterion to measure the final cumulative distance. Therefore, to weaken the dependence on the absolute value of RSSI and put emphasis on the trend comparison, we use the Pearson Coefficient to match the two RSSI curves. The Pearson Coefficient ρ of two continuous variables *(X,Y)* is calculated as follows:

$$\rho = \frac{\operatorname{cov}(X,Y)}{\sigma_X \sigma_Y} = \frac{\sum XY - \frac{\sum X \sum Y}{N}}{\sqrt{\left(\sum X^2 - \frac{(\sum X)^2}{N}\right)\left(\sum Y^2 - \frac{(\sum Y)^2}{N}\right)}}, \tag{17}$$

where $\operatorname{cov}(X,Y)$ is the covariance of *(X,Y)*, and N is the sequence length. $\rho \in [-1,1]$ represents the degree of correlation between X and Y, the larger the absolute value of ρ, the more relevant *(X,Y)* is.

As mentioned above, the value of v and Sf in Equation (6) vary with different people, the universality of the detection method should be considered. Moreover, we discover that the range of v usually is [0.6,1.4] m/s, while the range of Sf usually is [0.5,0.7] m. Thus, we cross-combine v taken from [0.6,1.4] in steps of 0.2 and Sf taken from [0.5,0.7] in steps of 0.02 to construct multiple theoretical RSSI curves for Pearson Coefficient calculation with the actual curve. After obtaining a series of ρ, (v_ρ, Sf_ρ) that corresponding to the largest $\rho_{\max}$ will be used for further judgement on the obstruction side if $\rho_{\max} \geq \delta$ (δ is the threshold, take 0.6 here), otherwise, the detection process of the current period D is terminated with the detection result as *in-room*.

5.4.2 Crest Comparison–based Matching on Obstruction Side. Since the signal propagation between the antenna on the obstruction side and the tag is seriously affected by the person, another novel curve matching method is proposed here to better aligning the fluctuations of the two curves. With the (v_ρ, Sf_ρ) obtained before, here we specify v is in $[v_\rho - 0.4, v_\rho + 0.4]$ with a step size of 0.2, Sf is in $[Sf_\rho - 0.04, Sf_\rho + 0.04]$ with a step size of 0.02, and construct the RSSI curves similarly. Then, compare each theoretical curve with the actual curve as follows until the matching one is found (*out-room*), or all fail to match (*in-room*):

- Filtering out the "small" crests in both curves. As shown in Figure 14, such tiny crests appearing in the curve should be combined or filtered directly, which can be realized by judging the amplitude difference between several crests and troughs. For example, the tiny crest

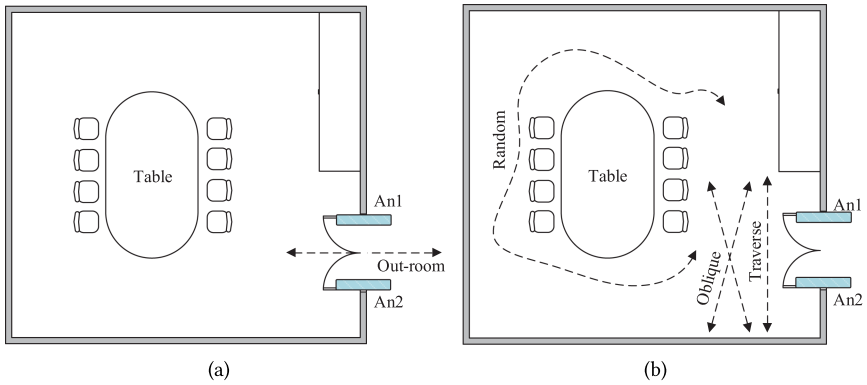

Fig. 15. Samples collection. (a) Out-room and (b) In-room.

of the leftmost case in Figure 14 can be located by the judgment: crest2 − trough $> \xi$ and crest1 − trough $\leq \xi$, ξ is the difference threshold.

- Panning the actual curve to align the first crest of the two curves.
- Comparing the occurrence time points of the two curve crests in sequence to find whether the difference is less than 250 ms. The matching is successful if all the time difference are eligible.

6 PERFORMANCE EVALUATION

6.1 Experimental Setup and Metrics

We implement a prototype of RF-AMOC based on COTS RFID devices with Impinj Speedway R420 reader, Laird S9028PCL antenna, and Alien 9640 tags. The tag is pasted in the lower right corner of the last page of the monitored file, and two opposite antennas are placed at the same height at the door to interrogate the tag.

To validate the robustness of the proposed system, we evaluate it in three typical environments with different widths of doors as 1.2 m, 0.9 m, and 1.8 m, recorded as meeting room, office and gate, respectively. A total of wight participants join the experiments (5 males and 3 females, 1.62–1.85 m tall) with a file holding in his/her hand. In all three environments, we ask all the volunteers to walk through the door (as shown in Figure 15(a)) 100 times while collecting the *out-room* samples. In regard to the *in-room* samples, the volunteers are requested to move in the room with the following three tracks 50 times for each (as shown in Figure 15(b)): (i) *Traverse,* (ii) *Oblique, and* (iii) *Random.*

To make the judgement targeted, the metrics used to evaluate the performance of RF-AMOC are given as follows:

- **Sensitivity** is the probability that the *out-room* is correctly classified.
- **Specificity** is the probability that the *in-room* is correctly classified.

6.2 Discussion on the Necessity of Two Antennas

We first prove the necessity of using two antennas for detection instead of using single antenna for one-sided signal change comparison. In the scheme of using the Pearson Coefficient for one side signal matching only, the antenna is always placed on the side of the tag. As shown in Figure 16, the sensitivity of the method that two antennas involved is 95%, which is a slight drop compared to 96.3% achieved by the one antenna method. However, introducing the second antenna significantly improve specificity from 69.6% to 94%, about 25% in increments. The reason behind this result is

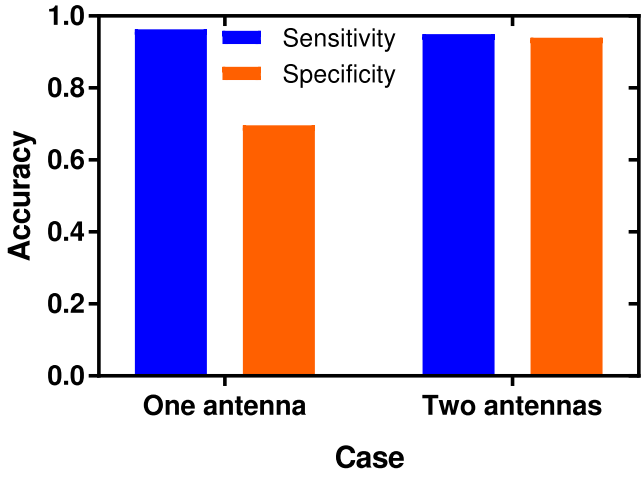

Fig. 16. Single antenna vs. Dual antenna.

that the addition of the second antenna is equivalent to an additional layer of restrictions, which greatly prevents the generation of false positives. Overall, the accuracy of the proposed method that leveraging two antennas is about 15% higher than that of using one antenna.

6.3 Comparison with Other Methods

To illustrate the effectiveness and robustness of the proposed method, the following two detection methods are selected, since they have already been successfully applied for false reading detection in the supply chain.

AD-SVM [28] is a feature extraction and classifier training–based detection method that is able to distinguish between the goods that actually pass through the RFID portal and the goods that are placed on the shelves. A total of 11 statistical features ([Max RSSI, Mean RSSI, RSSI variance, RSSI range, RSSI Skewness, RSSI Kurtosis, Phase variance, Phase range, Phase Skewness, Phase Kurtosis, Count]) are extracted from RSSI and phase to train the classifier. After verification in a real-world factory, SVM stood out in a number of machine learning algorithms with an accuracy rate of 95.3%.

DTW+DT [19] is a detection method based on time-series comparison leveraging DTW algorithm. The first step of it is to generate several reference time series using mean approach for both situations. Then the DTW distances between each time series and the reference series are calculated as the input to train a Decision Tree (DT) classification model. Finally, the category of the test time series can be derived according to its DTW distance from the reference series utilizing the trained model.

Based on the data collected in the meeting room, we divide the data with 70% training and 30% testing for the two comparison methods and obtain the identification accuracy in Figure 17. It can be found that AD-SVM performs best in resisting false negative with sensitivity of 98.2%. However, it provides specificity as low as 69.9%, which means AD-SVM tends to false alarm the *in-room* normal activity as *out-room*. The latter two methods based on time series have relatively better performance both in sensitivity and specificity. Specifically, DTW+DT achieves sensitivity of 93.3% and specificity of 91%, slightly lower than our method. The major cause for the low specificity of AD-SVM is that the *in-room* samples belonging to *Traverse* or *Oblique* are statistically similar to

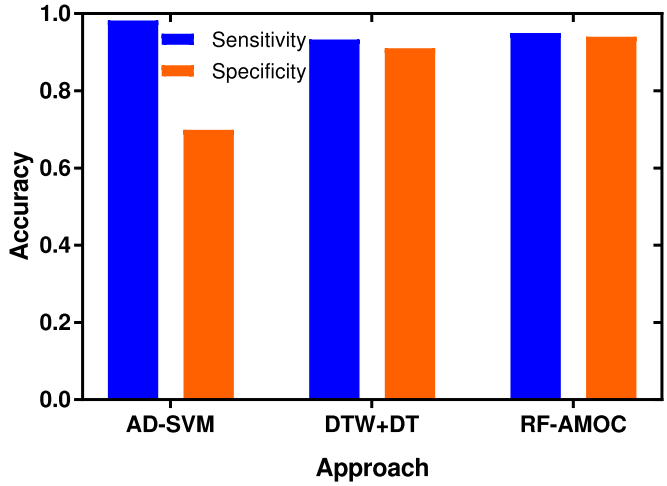

Fig. 17. Comparison with other methods.

(a) (b) (c)

Fig. 18. Experimental setup at the entrance of (a) meeting room, (b) office, and (c) gate.

the *out-room* ones, time-series-based comparisons can find differences not only in terms of RSSI values but also in the dimension of time.

6.4 Robustness Performance

6.4.1 Robustness to Environmental Differences. Because of the diversity of the usage scenarios, a system that performs well in one environment does not necessarily achieve the same performance in another environment, and the factor that has the greatest impact on identification performance is the size of the door. For example, the three typical scenarios including the meeting room, office and gate that involved in the experiment are shown in the Figure 18. The original models of AD-SVM and DTW+DT trained in the meeting room are directly tested in the office and the gate situations to demonstrate the environmental adaptability of the model, and the performance is shown in Figure 19. It can be clearly seen that because the models of AD-SVM and DTW+DT are trained in the meeting room, their performance drop significantly when moving to

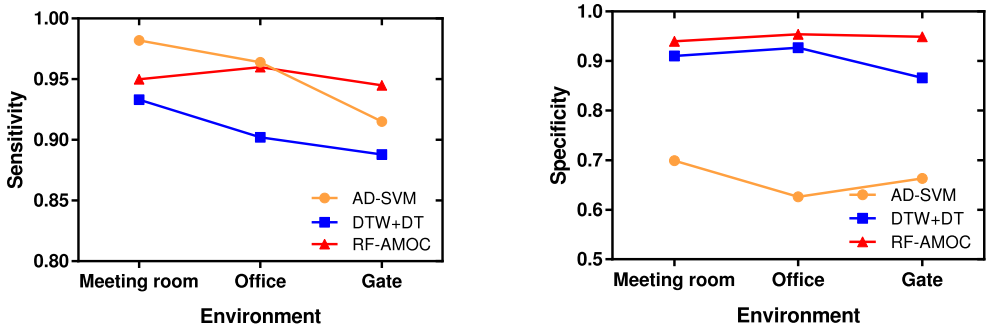

(a) (b)

Fig. 19. Accuracy distributions for cross-environment evaluation with (a) sensitivity and (b) specificity.

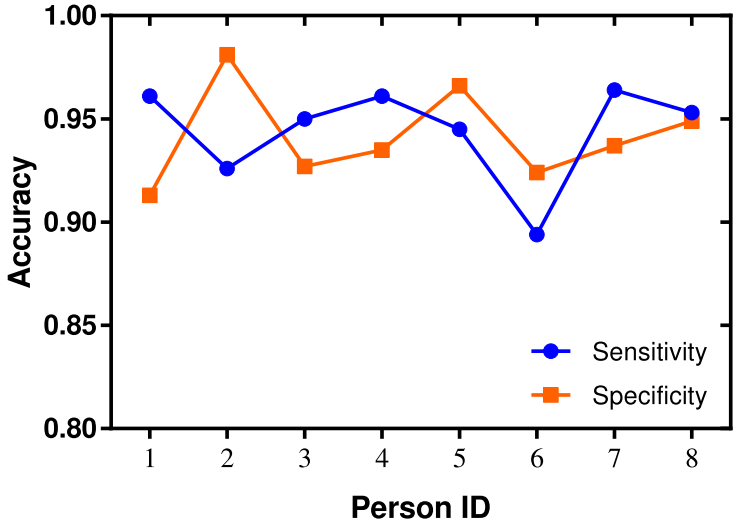

Fig. 20. Impact of individual difference on performance.

the office and gate for use. Especially for DTW+DT, its superior performance in the meeting room has disappeared here. Specifically, the sensitivity and specificity of AD-SVM are 96.4%, 62.6% in office, 91.5%, 66.3% in gate and the sensitivity and specificity of DTW+DT are 90.2%, 92.7% in office, 88.8%, 86.8% in gate, respectively. In contrast, our method can maintain a similar level of accuracy with the sensitivity of 96%, 94.5% and the specificity of 95.4%, 94.9% in two cases.

6.4.2 Robustness to Individual Differences. Considering the difference in speed and stride between people walking, the influence of individual differences on the performance of the system is also a factor that needs attention. Therefore, to clarify the impact of this factor on the three methods, the experimental results of the eight volunteers are shown in Figure 20. Our RSSI modeling and curve matching–based tag movement identification method shows good robustness in 8 people and preserves the overall accuracy of more than 90%. Particularly, the lowest sensitivity and specificity is 89.4%(volunteer 6), 91.3%(volunteer 1), while the highest sensitivity and specificity is 96.4%, 98.1%, respectively. To explore the reasons for the low sensitivity that less than 90%, we check the records and find that the height of volunteer 6 is 1.85 m. As a result, the swinging

amplitude of the arm and the stride will exceed the normal range due to such a high height, thus lowering the detection accuracy of RF-AMOC.

7 CONCLUSION

In this article, a lightweight RFID tag movement identification system (RF-AMOC) that does not require prior training is designed to solve the false reading issues for access management of carries. RF-AMOC provides a practical solution to effectively supervise the RFID tag equipped files and prevent unauthorized file carrying behavior through the opposite antennas placed at the door. We investigate the characteristics of the antenna variation with distance and angle to model the RSSI change patterns of antennas both on direct and obstruction side, which is the key innovations of our work. Based on the actual curve and the theoretical curve obtained from the modeling, we adopt the Pearson Coefficient and crest comparison method to match the two curves. Furthermore, a starting point acquisition method is proposed to better capture the meaningful time period for further identification. We implement RF-AMOC on COST RFID devices and evaluate it in different environments with various persons. Experimental results confirm the effectiveness and robustness of our system in both sensitivity and specificity, which achieves an average accuracy of greater than 94%.

Currently, we mainly consider the most common form when people carry the file out of the room, i.e., holding the file in one hand and going out normally with swing arms. Other situations such as holding in both hands, sandwiching under the armpit, and putting in a briefcase do not attract us too much attention. Although these situations are relatively simple compared to the case discussed in this article, they are also indispensable for a complete inspection system. Therefore, in future, we plan to improve the tag movement identification method for automatic tuning of detection schemes, and make it more robust to different forms of *out-room*. In addition, the communication between the tag and the antenna may be intentionally or unintentionally affected by the obstacle in daily use, especially when it is covered by the metal product. Thus, to further improve the robustness of the system, adopting the "metal-resistant" RFID tag seems to be a good solution, which can be achieved by attaching a magnetic absorbing material between the tag and the metal product or choosing the "strong" tag that designed specifically for use in extreme conditions.

REFERENCES

[1] 2012. IEEE standard for local and metropolitan area networks—Part 15.6: Wireless body area networks. *IEEE Std 802.15.6-2012* (Feb. 2012), 1–271.

[2] Yijian Bai, Fusheng Wang, and Peiya Liu. 2006. Efficiently filtering RFID data streams. In *Proceedings of the International VLDB Workshop on Clean Databases (Cleandb'06)*. 50–57.

[3] Gi Hwan Bong, Yoon Seok Chang, and Heun Oh Chang. 2014. A practical algorithm for reliability-based RFID event management considering warehouse operational environment. *Int. J. Adv. Log.* 3, 3 (2014), 100–108.

[4] J. Brusey, Mg Harrison, and C. Floerkemeier. 2003. Reasoning about uncertainty in location identification with auto-ID. *Automatic Identification Rfid Manufacturing* (2003).

[5] Wang Chen, Wei Wei, Hongzhi Lin, Hongbo Jiang, and John C. S. Lui. 2016. BLOW-UP: Toward distributed and scalable space filling curve construction in 3D volumetric WSNs. *ACM Trans. Sens. Netw.* 12, 4 (2016), 30.

[6] Tsan Ming Choi, Wing Kwan Yeung, T. C. Edwin Cheng, and Xiaohang Yue. 2018. Optimal scheduling, coordination, and the value of RFID technology in garment manufacturing supply chains. *IEEE Trans. Eng. Manage.*, 99 (2018), 1–13.

[7] Oscar Delgado-Mohatar, Amparo Fúster-Sabater, and José M. Sierra. 2011. A light-weight authentication scheme for wireless sensor networks. *Ad Hoc Netw.* 9, 5 (2011), 727–735.

[8] Xuming Fang, Nan Lei, Zonghua Jiang, and Lijun Chen. 2017. Noise-aware fingerprint localization algorithm for wireless sensor network based on adaptive fingerprint Kalman filter. *Comput. Netw.* 124 (2017), 97–107.

[9] T. Germa, F. Lerasle, N. Ouadah, and V. Cadenat. 2010. Vision and RFID data fusion for tracking people in crowds by a mobile robot. *Comput. Vis. Image Understand.* 114, 6 (2010), 641–651.

[10] Alexia Giannoula, Alba Gutierrezsacristán, Álex Bravo, Ferran Sanz, and Laura I. Furlong. 2018. Identifying temporal patterns in patient disease trajectories using dynamic time warping: A population-based study. *Sci. Rep.* 8, 1 (2018), 4216.

[11] M. Goller, C. Feichtenhofer, and A. Pinz. 2014. *Fusing RFID and Computer Vision for Probabilistic Tag Localization.* 89–96 pages.

[12] Ding Han, Jinsong Han, Longfei Shangguan, Xi Wei, Zhiping Jiang, Yang Zheng, Zimu Zhou, Panglong Yang, and Ji Zhong Zhao. 2017. A platform for free-weight exercise monitoring with passive tags. *IEEE Trans. Mobile Comput.*, 99 (2017), 1–1.

[13] J. [3]. Han and M. Kamber. 2005. *Data Mining: Concepts and Technique.*

[14] Matthias Hauser, Daniel Z¨gner, Christoph M. Flath, and Frédéric Thiesse. 2015. Pushing the limits of RFID: Empowering RFID-based electronic article surveillance with data analytics techniques. In *Proceedings of the International Conference on Information Systems.*

[15] Wei Qing Huang, Chang Ding, Si Ye Wang, Junyu Lin, Shao Yi Zhu, and Yue Cui. 2017. Design and realization of an indoor positioning algorithm based on differential positioning method. In *Proceedings of the International Conference on Wireless Algorithms, Systems, and Applications.* 546–558.

[16] C. Jiang, Y. He, X. Zheng, and Y. Liu. 2018. Orientation-aware RFID tracking with centimeter-level accuracy. In *Proceedings of the 17th ACM/IEEE International Conference on Information Processing in Sensor Networks (IPSN'18).* 290–301.

[17] Yu Ju Tu and Selwyn Piramuthu. 2008. Reducing false reads in RFID-embedded supply chains. *J. Theor. Appl. Electr. Comm. Res.* 3, 2 (2008), 60–70.

[18] Thorben Keller and Elgar Fleisch. 2014. *Classification Models for RFID-Based Real-Time Detection of Process Events in the Supply Chain: An Empirical Study.* ACM.

[19] Thorben Keller, Frédéric Thiesse, and Elgar Fleisch. 2014. Using dynamic time warping to identify RFID tag movement in a logistics scenario with and without additional process knowledge. (2014).

[20] T. Keller, F. Thiesse, A. Ilic, and E. Fleisch. 2013. Decreasing false-positive RFID tag reads by improved portal antenna setups. In *Internet of Things.* 99–106.

[21] Thorben Keller, Frédéric Thiesse, Jens Kungl, and Elgar Fleisch. 2010. Using low-level reader data to detect false-positive RFID tag reads. In *Internet of Things.* 1–8.

[22] Yudai Komori, Kazuya Sakai, and Satoshi Fukumoto. 2018. Fast and secure tag authentication in large-scale RFID systems using skip graphs aî. *Comput. Commun.* 116 (2018), 77–89.

[23] LaurieDavies and UrsulaGather. 1993. The identification of multiple outliers. *Publ. Am. Stat. Assoc.* 88, 423 (1993), 782–792.

[24] Laurie Davies and Ursula Gather. 1993. The identification of multiple outliers. *J. Am. Stat. Assoc.* 88, 423 (1993), 782–792.

[25] Xie Lei, Chuyu Wang, Alex X. Liu, Jianqiang Sun, and Sanglu Lu. 2018. Multi-touch in the air: Concurrent micro-movement recognition using RF signals. *IEEE/ACM Trans. Netw.*, 99 (2018), 1–14.

[26] Tao Li, Shigang Chen, and Yibei Ling. 2013. Efficient protocols for identifying the missing tags in a large RFID system. *IEEE/ACM Trans. Netw.* 21, 6 (2013), 1974–1987.

[27] T. Liu, L. Yang, Q. Lin, Y. Guo, and Y. Liu. 2014. Anchor-free backscatter positioning for RFID tags with high accuracy. In *Proceedings of the IEEE Conference on Computer Communications (INFOCOM'14).* 379–387.

[28] Haishu Ma, Yi Wang, and Kesheng Wang. 2018. Automatic detection of false positive RFID readings using machine learning algorithms. *Expert Syst. Appl.* 91 (2018).

[29] Martin Mayer and Norbert Goertz. 2016. RFID tag acquisition via compressed sensing: Fixed vs. random signature assignment. *IEEE Trans. Wireless Commun.* 15, 3 (2016), 2118–2129.

[30] Lionel M. Ni, Yunhao Liu, Yiu Cho Lau, and Abhishek P. Patil. 2004. LANDMARC: Indoor location sensing using active RFID. 10, 6 (2004), 701–710.

[31] Saiyu Qi, Yuanqing Zheng, Mo Li, Yunhao Liu, and Jinli Qiu. 2016. Scalable industry data access control in RFID-enabled supply chain. *IEEE/ACM Trans. Netw.* 24, 6 (2016), 3551–3564.

[32] L. Qiu, X. Liang, and Z. Huang. 2017. PATL: A RFID tag localization based on phased array antenna. *Sci. Rep.* 7 (2017), 44183.

[33] Mark Roberti. 2004. EPCglobal ratifies Gen 2 standard. *RFID J.* 16 (2004).

[34] A. P. Sample, C. Macomber, Liang Ting Jiang, and J. R. Smith. 2016. Optical localization of passive UHF RFID tags with integrated LEDs. In *Proceedings of the IEEE International Conference on RFID.*

[35] L. Shangguan, Z. Yang, A. X. Liu, Z. Zhou, and Y. Liu. 2017. STPP: Spatial-temporal phase profiling-based method for relative RFID tag localization. *IEEE/ACM Trans. Netw.* 25, 1 (2017), 596–609.

[36] Rudranshu Sharma and Ankur Singh Bist. 2015. Machine learning: A survey. *Int. J. Eng. Sci. Res. Technol.* 4, 3 (2015).

[37] Chuyu Wang, Lei Xie, Wei Wang, Yingying Chen, Yanling Bu, and Sanglu Lu. 2018. RF-ECG: Heart rate variability assessment based on COTS RFID tag array. *Proc. ACM Interact. Mobile Wear. Ubiq. Technol.* 2, 07 (2018), 1–26. DOI: https://doi.org/10.1145/3214288

[38] Gu Yu, Jinhai Zhan, Yusheng Ji, Li Jie, and Shangbing Gao. 2017. MoSense: A RF-based motion detection system via off-the-shelf WiFi devices. *IEEE IofT J.*, 99 (2017), 1–1.

[39] Wang Zhongqin, Xu Min, Ye Ning, Wang Ruchuan, and Huang Haiping. 2019. Computer vision-assisted region-of-interest RFID tag recognition and localization in multipath-prevalent environments. *Proc. ACM Interact. Mobile Wear. Ubiq. Technol.* 3, 29 (2019), 1–30.

[40] Dali Zhu, Bobai Zhao, and Siye Wang. 2018. Mobile target indoor tracking based on multi-direction weight position Kalman filter. *Comput. Netw.* 141 (2018), 115–127.

[41] Shaoyi Zhu, Siye Wang, Fangtao Zhang, Yanfang Zhang, Yue Feng, and Weiqing Huang. 2018. Environmentally adaptive real-time detection of RFID false readings in a new practical scenario. In *Proceedings of the 2018 IEEE SmartWorld, Ubiquitous Intelligence & Computing, Advanced & Trusted Computing, Scalable Computing & Communications, Cloud & Big Data Computing, Internet of People and Smart City Innovation (SmartWorld/SCALCOM/UIC/ATC/CBDCom/IOP/SCI'18)*. 338–345.

Received May 2019; revised April 2020; accepted May 2020